MJFAS MALAYSIAN JOURNAL OF FUNDAMENTAL AND APPLIED SCIENCES
PRINT ISSN: 2289-5981 | ONLINE ISSN: 2289-599X

RESEARCH ARTICLE

Free convection boundary layer flow on a solid sphere in a nanofluid with viscous dissipation

Muhammad Khairul Anuar Mohamed [a,*], Nor Aida Zuraimi Md Noar [b], Mohd Zuki Salleh [b], Anuar Ishak [c]

[a] *Faculty of Engineering Technology, DRB-HICOM University of Automotive Malaysia, Peramu Jaya Industrial Area, 26607 Pekan, Pahang, Malaysia*
[b] *Applied & Industrial Mathematics Research Group, Faculty of Industrial Sciences and Technology, Universiti Malaysia Pahang, 26300 UMP Kuantan, Pahang, Malaysia*
[c] *School of Mathematical Sciences, Faculty of Science & Technology, Universiti Kebangsaan Malaysia, 43600 UKM Bangi, Selangor, Malaysia*

* *Corresponding author: khairul.anuar@dhu.edu.my*

Article history
Received 3 June 2018
Revised 2 August 2018
Accepted 13 September 2018
Published Online 25 June 2019

Abstract

Present study considers the mathematical model of free convection boundary layer flow and heat transfer in a nanofluid over a solid sphere with viscous dissipation effect. The transformed partial differential equations are solved numerically using the Keller-box method. The numerical values for the reduced Nusselt number, reduced Sherwood number and the reduced local skin friction coefficient are obtained, as well as concentration profiles, temperature profiles and velocity profiles are illustrated graphically. Effects of the pertinent parameters, which are the Prandtl number, buoyancy ratio parameter, Brownian motion parameter, thermophoresis parameter, Lewis number and Eckert number are analyzed and discussed. It is found that the increase of Brownian motion parameter promoted the reduce of concentration boundary layer thickness while thermophoresis parameter did oppositely. It is worth mentioning that the results reported here are important for the researchers working in this area which can be used as a reference and comparison purposes in the future.

Keywords: Free convection, nanofluid, solid sphere, viscous dissipation

INTRODUCTION

Nanofluid is a based fluid which contains nanoparticles, for example $Ti0_2$, Al_20_3 and CuO. Nanofluid is well known and proven in enhancing the thermal conductivity, viscosity, thermal diffusivity and convective heat transfer compared to its based fluids such as water or oil (Wong and De Leon, 2010). Further, the small amount of nanoparticles that immersed in a nanofluid can reduce the chances of sedimentation and also minimize the rate of erosion onto component surface. Therefore, there will be less or no damaging which can prolong the life time onto component. Besides, less sedimentation means no clogging and this characteristic will specialize nanofluid to be employed in microchannel applications, for example in automotive turbocharger cooling system (Mohamed, 2017).

Nanofluid is employed in many applications, for example in industries as a coolant medium in tyre production, in automotives as a coolant in car radiator, brake fluid and fuel catalyst to improve engine combustion, in medicines as a drug vehicle for cancer therapeutics and also acts to cool the microchip in electronic devices (Wong and De Leon, 2010). The widely contributions have attracted many researchers to investigate the convective flow in a nanofluid as done recently by Anwar et al. (2016), Khan (2017), Kho et al. (2017), Mohamed et al. (2016; 2018), Abro et al. (2018) and Gul et al. (2018).

The boundary layer flow on a solid sphere is applied in many industrial applications, such as the spherical storage tanks, turbocharged ball bearing in automotives, the packed beds in a chemical reactor or distillation process and in many electronic components that nearly spherical. Chiang et al. (1964) are the first who analyzed the free convection on a sphere where the laminar flow is considered. Amato and Tien (1972) have done the experimental studies on isothermal spheres in water. The experimental results showed a very good agreement with predictions of Acrivos' theory. Lien and Chen (1986) done the analysis on forced convection flow on a permeable sphere while Huang and Chen (1987) investigated this topic with the effects of suction and blowing. Next, Jafarpur and Yovanovich (1992) and Jia and Gogos (1996) solved the problem of laminar free convective from an isothermal sphere by using false transient algorithm and the new analytical method, respectively. This problem is then extended to other types of fluid like micropolar fluid by Nazar et al. (2002a; 2002b) and Alkasasbeh et al. (2014a; 2014b), Bingham plastic by Nalluri et al. (2015), while Kasim et al. (2013) and Abdul Gaffar et al. (2015) covered the viscoelastic fluid. Next, the mixed convection around a heated and cooled sphere is investigated by Gopmandal and Bhattacharyya (2011). It is found that the heated sphere delays the flow separation and enhances the drag coefficient as well as the rate of heat transfer. Further, the convective flow on a solid sphere with Newtonian heating is investigated by Salleh et al. (2010; 2012).

In all investigations mentioned above, the viscous dissipation effects are neglected. The viscous dissipation may be described as the induced kinetic energy from body that is converted into thermal energy. It is usually presented in free convection with large deccelarations from high rotating speeds and also in highly viscous flow with moderate velocity (Gebhart, 1962). Recent investigations on viscous dissipation effects are including the works by Mabood et al. (2016), Ugur Akbulut et al. (2017) and Zokri et al. (2017; 2018).

Inspired by the given literatures, present study objective is to solve the free convective boundary layer flow on a solid sphere in a nanofluid with viscous dissipation effects. The effects of nanoparticle random motion in nanofluid, temperature diffusivity and ratio between the temperature diffusivity over mass diffusivity are interest phenomenas considered. Therefore, the nanofluid Buongiorno-Darcy model is suitable to be applied (Buongiorno, 2006). From the best of our knowledge, this problem especially related to viscous dissipation effect is never been discussed before, hence the reported results are new.

MATHEMATICAL FORMULATIONS

The solid sphere with radius a, which is heated to a constant temperature T_w embedded in a nanofluid with ambient temperature T_∞ is considered. The physical model is shown in Fig 1. The orthogonal coordinates of $\bar{x}$ are measured along the sphere surface, starting from the lower stagnation point $\bar{x}=0$, and $\bar{y}$ measures the distance normal from the surface. $\bar{r}(\bar{x}) = a\sin\left(\frac{\bar{x}}{a}\right)$ is the radial distance from the symmetrical axis to the sphere surface. The suggested dimensional governing equations according to Nazar et al. (2002a) and Salleh et al. (2010) are:

$$\frac{\partial}{\partial \bar{x}}(\bar{r}\,\bar{u}) + \frac{\partial}{\partial \bar{y}}(\bar{r}\,\bar{v}) = 0, \tag{1}$$

$$\bar{u}\frac{\partial \bar{u}}{\partial \bar{x}} + \bar{v}\frac{\partial \bar{u}}{\partial \bar{y}} = \nu\frac{\partial^2 \bar{u}}{\partial \bar{y}^2} + g\beta(T-T_\infty)\sin\frac{\bar{x}}{a} + g\beta_c(C-C_\infty)\sin\frac{\bar{x}}{a}. \tag{2}$$

$$\bar{u}\frac{\partial T}{\partial \bar{x}} + \bar{v}\frac{\partial T}{\partial \bar{y}} = \alpha\frac{\partial^2 T}{\partial \bar{y}^2} + \tau\left[D_B\frac{\partial C}{\partial \bar{y}}\frac{\partial T}{\partial \bar{y}} + \frac{D_T}{T_\infty}\left(\frac{\partial T}{\partial \bar{y}}\right)^2\right] + \frac{\mu}{\rho C_p}\left(\frac{\partial \bar{u}}{\partial \bar{y}}\right)^2, \tag{3}$$

$$\bar{u}\frac{\partial C}{\partial \bar{x}} + \bar{v}\frac{\partial C}{\partial \bar{y}} = D_B\frac{\partial^2 C}{\partial \bar{y}^2} + \frac{D_T}{T_\infty}\frac{\partial^2 T}{\partial \bar{y}^2}, \tag{4}$$

subject to the boundary conditions

$$\begin{gathered}\bar{u}(\bar{x},0) = \bar{v}(\bar{x},0) = 0,\ T(\bar{x},0) = T_w,\ C(\bar{x},0) = C_w,\\ \bar{u}(\bar{x},\infty)\to 0,\ T(\bar{x},\infty)\to T_\infty,\ C(\bar{x},\infty)\to C_\infty\end{gathered} \tag{5}$$

where $\bar{u}$ and $\bar{v}$ are the velocity components along the $\bar{x}$ and $\bar{y}$ axes, respectively, μ is the dynamic viscosity, ν is the kinematic viscosity, g is the gravity acceleration, β and β_c are the thermal and concentration expansion coefficients, T is the local temperature, ρ is the fluid density and C_p is the specific heat capacity at a constant pressure. Furthermore, C is the nanoparticle volume fraction, C_w and C_∞ are the surface and ambient nanoparticle volume fraction respectively.

The Eqs. (1)-(4) are in dimensional form and will transform to non-dimensional. Then, the following non-dimensional variables are introduced:

$$\begin{gathered}x = \frac{\bar{x}}{a},\quad y = Gr_x^{1/4}\frac{\bar{y}}{a},\quad u = \frac{a}{\nu}Gr_x^{-1/2}\bar{u},\quad v = \frac{a}{\nu}Gr_x^{-1/4}\bar{v},\\ r = \frac{\bar{r}}{a},\quad \theta(\eta) = \frac{T-T_\infty}{T_w-T_\infty},\quad \phi(\eta) = \frac{C-C_\infty}{C_w-C_\infty}.\end{gathered} \tag{6}$$

where θ and ϕ are the rescaled dimensionless temperature and nanoparticle volume fraction of the fluid and $Gr_x = \frac{g\beta(T_w-T_\infty)a^3}{\nu^2}$ is the Grashof number. Using Eq. (6), Eqs. (1)-(4) become

$$\frac{\partial}{\partial x}(ru) + \frac{\partial}{\partial y}(rv) = 0, \tag{7}$$

$$u\frac{\partial u}{\partial x} + v\frac{\partial u}{\partial y} = \frac{\partial^2 u}{\partial y^2} + \theta\sin x + \frac{g\beta_c(C_w-C_\infty)a^3}{\nu^2 Gr_x}\phi\sin x, \tag{8}$$

$$u\frac{\partial \theta}{\partial x} + v\frac{\partial \theta}{\partial y} = \frac{1}{\Pr}\frac{\partial^2 \theta}{\partial y^2} + N_b\frac{\partial \phi}{\partial y}\frac{\partial \theta}{\partial y} + N_t\left(\frac{\partial \theta}{\partial y}\right)^2 + Ec\left(\frac{\partial u}{\partial y}\right)^2, \tag{9}$$

$$u\frac{\partial \phi}{\partial x} + v\frac{\partial \phi}{\partial y} = \frac{D_B}{\nu}\frac{\partial^2 \phi}{\partial y^2} + \frac{D_T(T_w-T_\infty)}{T_\infty\nu(C_w-C_\infty)}\frac{\partial^2 \theta}{\partial y^2} \tag{10}$$

where $\Pr = \frac{\nu}{\alpha}$ is the Prandtl number, $N_b = \frac{\tau D_B(C_w-C_\infty)}{\nu}$ is the Brownian motion parameter, $N_t = \frac{\tau D_T(T_w-T_\infty)}{T_\infty\nu}$ is the thermophoresis parameter and $Ec = \frac{\nu^2 Gr_x}{a^2 C_p(T_w-T_\infty)}$ is the Eckert number. Notice that $\mu = \rho\nu$, the boundary conditions (5) become

$$\begin{gathered}u(x,0)=0,\ v(x,0)=0,\ \theta(x,0)=1,\ \phi(x,0)=1,\\ u(x,\infty)\to 0,\ \theta(x,\infty)\to 0,\ \phi(x,\infty)\to 0\end{gathered} \tag{11}$$

In order to solve the partial differential Eqs. (7)-(10), the following functions are introduced:

$$\psi = x r(x) f(x,y),\ \ \phi = \phi(x,y),\ \ \theta = \theta(x,y), \tag{12}$$

where ψ is the stream function defined as $u = \frac{1}{r}\frac{\partial \psi}{\partial y}$ and $v = -\frac{1}{r}\frac{\partial \psi}{\partial x}$ which identically satisfies Eq. (7). Substituting Eq. (12) into Eqs. (7)-(10), the following partial differential equations are obtained:

$$\begin{gathered}\frac{\partial^3 f}{\partial y^3} + \left(1+\frac{x}{\sin x}\cos x\right)f\frac{\partial^2 f}{\partial y^2} - \left(\frac{\partial f}{\partial y}\right)^2 + (\theta+\chi\phi)\frac{\sin x}{x}\\ = x\left(\frac{\partial f}{\partial y}\frac{\partial^2 f}{\partial x\partial y} - \frac{\partial f}{\partial x}\frac{\partial^2 f}{\partial y^2}\right).\end{gathered} \tag{13}$$

$$\begin{gathered}\frac{1}{\Pr}\frac{\partial^2 \theta}{\partial y^2} + \left(1+\frac{x}{\sin x}\cos x\right)f\frac{\partial \theta}{\partial y} + N_b\frac{\partial \phi}{\partial y}\frac{\partial \theta}{\partial y} + N_t\left(\frac{\partial \theta}{\partial y}\right)^2\\ = x\left(\frac{\partial f}{\partial y}\frac{\partial \theta}{\partial x} - \frac{\partial f}{\partial x}\frac{\partial \theta}{\partial y} - xEc\left(\frac{\partial^2 f}{\partial y^2}\right)^2\right),\end{gathered} \tag{14}$$

$$\begin{gathered}\frac{\partial^2 \phi}{\partial y^2} + \frac{N_t}{N_b}\frac{\partial^2 \theta}{\partial y^2} + \left(1+\frac{x}{\sin x}\cos x\right)Lef\frac{\partial \phi}{\partial y}\\ = xLe\left(\frac{\partial f}{\partial y}\frac{\partial \phi}{\partial x} - \frac{\partial f}{\partial x}\frac{\partial \phi}{\partial y}\right),\end{gathered} \tag{15}$$

where $Le = \frac{\nu}{D_B}$ and $\chi = \frac{Gr_c}{Gr_x}$ are the Lewis number and the buoyancy ratio parameter, respectively. Notice that $Gr_c = \frac{g\beta_c(C_w-C_\infty)a^3}{\nu^2}$ is the mass transfer Grashof number. The boundary conditions (11) become

$$\begin{gathered}f(x,0) = \frac{\partial f}{\partial y}(x,0) = 0,\ \theta(x,0)=1,\ \phi(x,0)=1,\\ \frac{\partial f}{\partial y}(x,\infty)\to 0,\ \theta(x,\infty)\to 0,\ \phi(x,\infty)\to 0\end{gathered} \tag{16}$$

The skin friction coefficient C_f, the local Nusselt number Nu_x and the local Sherwood number Sh_x are given by

$$C_f = \frac{\tau_w}{\rho U_\infty^2},\ Nu_x = \frac{aq_w}{k(T_w - T_\infty)},\ Sh_x = \frac{aj_w}{D_B(C_w - C_\infty)}. \tag{17}$$

and the surface shear stress τ_w, the surface heat flux q_w and the surface mass flux j_w are given by

$$\tau_w = \mu\left(\frac{\partial \bar{u}}{\partial \bar{y}}\right)_{\bar{y}=0},\quad q_w = -k\left(\frac{\partial T}{\partial \bar{y}}\right)_{\bar{y}=0},\quad j_w = -D_B\left(\frac{\partial C}{\partial \bar{y}}\right)_{\bar{y}=0}, \tag{18}$$

with k being the thermal conductivity, respectively. Substituting Eq. (6), (12) and (18) into Eq. (17) gives

$$C_f Gr_x^{1/4} = \left(x\frac{\partial^2 f}{\partial y^2}\right)_{\bar{y}=0},\quad Nu_x Gr_x^{-1/4} = -\left(\frac{\partial \theta}{\partial y}\right)_{\bar{y}=0}$$
$$\text{and}\quad Sh_x Gr_x^{-1/4} = -\left(\frac{\partial \phi}{\partial y}\right)_{\bar{y}=0}. \tag{19}$$

Table 1 Comparison values of $Nu_x Gr_x^{-1/4}$ with previous published results for various values of x when $\Pr = 0.7, N_b = N_t = \chi = Ec = Le = 0$.

x	Huang and Chen (1987)	Nazar et al. (2002a)	Salleh et al. (2010)	Present
0	0.4574	0.4576	0.4576	0.4576
$\pi/18$	0.4563	0.4565	0.4565	0.4565
$\pi/9$	0.4532	0.4533	0.4533	0.4533
$\pi/6$	0.4480	0.4480	0.4481	0.4480
$2\pi/9$	0.4407	0.4405	0.4406	0.4406
$5\pi/18$	0.4312	0.4308	0.4310	0.4310
$\pi/3$	0.4194	0.4198	0.4195	0.4195
$7\pi/18$	0.4053	0.4046	0.4053	0.4053
$4\pi/9$	0.3886	0.3879	0.3886	0.3886
$\pi/2$	0.3694	0.3684	0.3692	0.3692
$5\pi/9$			0.3470	0.3469
$11\pi/18$			0.3216	0.3215
$2\pi/3$			0.2925	0.2925
$13\pi/18$				0.2594
$7\pi/9$				0.2216
$5\pi/6$				0.1795
$8\pi/9$				0.1265
$17\pi/18$				0.0712

NUMERICAL METHOD

The partial differential equations (13) to (15) subjected to boundary conditions (16) were solved numerically using the Keller-box method, which is an implicit finite difference method in conjunction with Newton's method for linearization, making it suitable to solve parabolic partial differential equations at any order. As described in the books by Na (1979) and Mohamed (2018), this method started by transforming the system of Eqs. (13) to (15) to a first order system. The finite difference method was taken part and linearized by using Newtons method. The resulting algebraic equations were written in matrix vector form and finally solved the linear system by the block tridiagonal elimination technique.

RESULTS AND DISCUSSION

The Keller-box algorithms were coded in MATLAB software and computed numerically, with variation values of six parameters, namely the Prandtl number $\Pr$, the buoyancy ratio parameter χ, the Brownian motion parameter N_b, the thermophoresis parameter N_t, the Lewis number Le and the Eckert number Ec. The boundary layer thickness $y_\infty = 8$ and step size $\Delta y = 0.02$, $\Delta x = 0.005$ were used in obtaining the numerical results. From numerical calculation, it is understood that the numerical results obtained are rarely to be laminar until the end of sphere. The boundary layer flow will has separation usually after $x = 2\pi/3$ as reported previously by Huang and Chen (1987), Nazar et al. (2002a) and Salleh et al. (2010). For comparison purposes, Table 1 shows the comparison values with previous published results. The numerical results are updated to the end of sphere $(x = \pi)$. It is found that the results are in a good agreement and it is believed that Keller-box method is very efficient in solving the convective boundary layer problems involving the reduced partial differential equations.

Table 2 Values of $Nu_x Gr_x^{-1/4}$ for various values of Ec and x when $\Pr = 1$, $N_b = N_t = \chi = 0.1$ and $Le = 10$.

$x\,/\,Ec$	0	0.1	0.2	1
0	0.5310	0.5310	0.5310	0.5310
$\pi/18$	0.5297	0.5285	0.5274	0.5182
$\pi/9$	0.5261	0.5215	0.5169	0.4799
$\pi/6$	0.5202	0.5100	0.4998	0.4171
$2\pi/9$	0.5118	0.4942	0.4766	0.3316
$5\pi/18$	0.5009	0.4744	0.4478	0.2249
$\pi/3$	0.4874	0.4510	0.4151	0.1038
$7\pi/18$	0.4723	0.4406	0.3774	
$4\pi/9$	0.4531	0.3954	0.3364	
$\pi/2$	0.4313	0.3632	0.2931	
$5\pi/9$	0.4064	0.3287	0.2484	
$11\pi/18$	0.3780	0.2922	0.2032	
$2\pi/3$	0.3457	0.2539	0.1582	
$13\pi/18$	0.3090	0.2243	0.1144	
$7\pi/9$	0.2668	0.1722	0.0728	
$5\pi/6$	0.2180	0.1290	0.0352	
$8\pi/9$	0.1605	0.0848	0.0047	
$17\pi/18$	0.0928	0.0419		

Table 3 Values of $Sh_x Gr_x^{-1/4}$ for various values of Ec and x when $\Pr = 1$, $N_b = N_t = \chi = 0.1$ and $Le = 10$.

x / Ec	**0**	**0.1**	**0.2**	**1**
0	1.2198	1.2198	1.2198	1.2198
$\pi/18$	1.2170	1.2181	1.2192	1.2275
$\pi/9$	1.2087	1.2130	1.2172	1.2512
$\pi/6$	1.1950	1.2043	1.2136	1.2895
$2\pi/9$	1.1756	1.1917	1.2079	1.3406
$5\pi/18$	1.1505	1.1748	1.1992	1.4027
$\pi/3$	1.1196	1.1530	1.1872	1.4708
$7\pi/18$	1.0848	1.1427	1.1701	
$4\pi/9$	1.0404	1.0931	1.1468	
$\pi/2$	0.9903	1.0525	1.1162	
$5\pi/9$	0.9330	1.0037	1.0764	
$11\pi/18$	0.8676	0.9454	1.0259	
$2\pi/3$	0.7933	0.8761	0.9623	
$13\pi/18$	0.7086	0.8165	0.8830	
$7\pi/9$	0.6117	0.6960	0.7844	
$5\pi/6$	0.4996	0.5783	0.6610	
$8\pi/9$	0.3677	0.4340	0.5039	
$17\pi/18$	0.2124	0.2564		

Table 4 Values of $C_f Gr_x^{1/4}$ for various values of Ec and x when $\Pr = 1$, $N_b = N_t = \chi = 0.1$ and $Le = 10$.

x / Ec	**0**	**0.1**	**0.2**	**1**
0	0.0000	0.0000	0.0000	0.0000
$\pi/18$	0.1068	0.1068	0.1068	0.1068
$\pi/9$	0.2116	0.2117	0.2118	0.2124
$\pi/6$	0.3127	0.3129	0.3132	0.3154
$2\pi/9$	0.4081	0.4087	0.4093	0.4143
$5\pi/18$	0.4962	0.4973	0.4985	0.5079
$\pi/3$	0.5753	0.5771	0.5768	0.5922
$7\pi/18$	0.6420	0.6462	0.6475	
$4\pi/9$	0.6990	0.7027	0.7066	
$\pi/2$	0.7427	0.7476	0.7526	
$5\pi/9$	0.7720	0.7780	0.7842	
$11\pi/18$	0.7855	0.7927	0.8000	
$2\pi/3$	0.7819	0.7900	0.7982	
$13\pi/18$	0.7593	0.7756	0.7769	
$7\pi/9$	0.7147	0.7236	0.7327	
$5\pi/6$	0.6426	0.6511	0.6599	
$8\pi/9$	0.5317	0.5390	0.5465	
$17\pi/18$	0.3068	0.3656		

Tables 2 to 4 present the values of $Nu_x Gr_x^{-1/4}, Sh_x Gr_x^{-1/4}$ and $C_f Gr_x^{1/4}$ against x with various values of Ec. From Tables 2 and 3, it is found that the values of $Nu_x Gr_x^{-1/4}$ and $Sh_x Gr_x^{-1/4}$ decreased as x increased. This is physically the sign of reduction in convective heat and mass transfer capability which promotes the conduction of heat transfer. Further, the decreases in both quantities are small at the beginning, this situation turns more significantly as x increases to the end of the sphere. This may be explained as follow; at high value of x, especially as x increases to the end of sphere, the influence of gravity acceleration onto the nanofluid comes in contact with sphere surface has promoted the conduction of heat and mass transfer to be dominant than the convection. This situation is contradicted at the beginning of the sphere where the gravity acceleration role on nanofluid and surface engagement is negligible, hence enhancing the convection heat and mass transfer process rather than conduction.

Meanwhile, the increase at the beginning of sphere gives rise on the value of $C_f Gr_x^{1/4}$. This situation becomes contrast at the middle of the sphere where $C_f Gr_x^{1/4}$ decreases marginally and turns drastically at the end of sphere. Further, by considering the effects of viscous dissipation effects on the quantities of interest, it is found that the increase of Ec results in the increase of $C_f Gr_x^{1/4}$ and $Sh_x Gr_x^{-1/4}$ while $Nu_x Gr_x^{-1/4}$ decreases. In addition, it is noticed that the increase of Ec promotes the flow separation.

Figs. 2 and 4 show the temperature profile $\theta(\eta)$ at a stagnation region $(x = 0)$ for various values of $\Pr, N_b, N_t, Le$ and χ, respectively. It was found that the increase of Pr in Figure 2 resulted in the decrease of thermal boundary layer thickness while Le did oppositely. It is due to a decrease in thermal diffusivity which leads to the reduction in energy ability that reduces the thermal boundary layer thickness as Pr increases. In Figs. 3 and 4, the changes in parameters N_b, N_t and χ did not give much effect on the thermal boundary layer thickness. The temperature gradient was slightly increased as χ was increased, while was decreased as N_b and N_t were increased.

The velocity profiles $f'(\eta)$ at a stagnation region $(x = 0)$ for various values of $\Pr, N_b, N_t$ and Le are illustrated in Figs. 5 and 6. It is suggested that the increase of Le and Pr results in a decrease of $f'(\eta)$ and the velocity gradient. The increase of Pr physically increases the fluid viscosity and becomes sticky between fluid molecules which results in the decreasing in velocity. The trends were contradicted in Fig. 6 where the increase of N_b and N_t raised the $f'(\eta)$ and the velocity gradient.

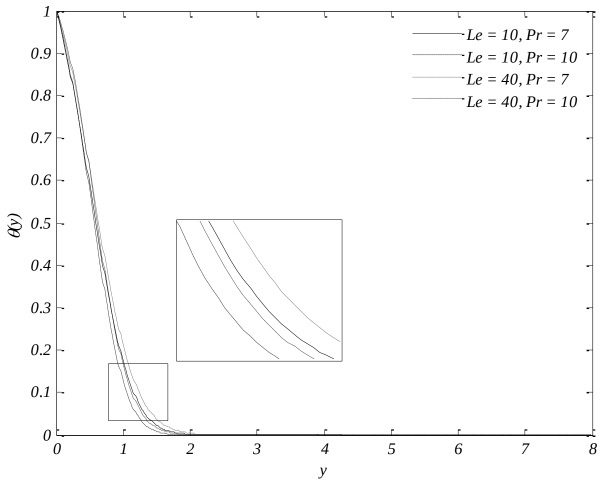

Fig. 2 Temperature profiles $\theta(y)$ against y for various values of Pr and Le when $N_b = N_t = \chi = Ec = 0.1$.

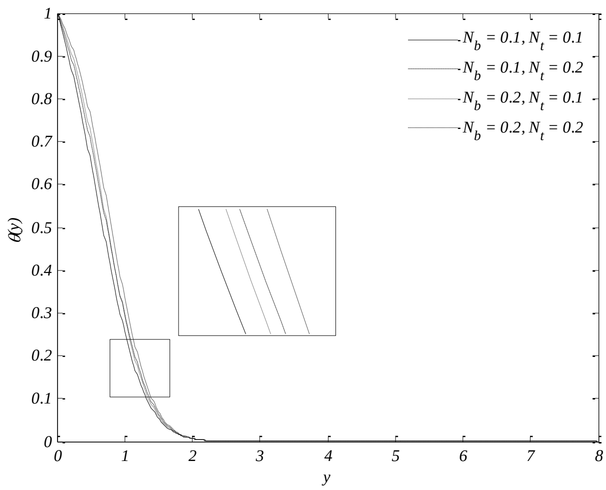

Fig. 3 Temperature profiles $\theta(y)$ against y for various values of values of N_b and N_t when $\Pr = 7$, $Le = 10$ and $\chi = Ec = 0.1$.

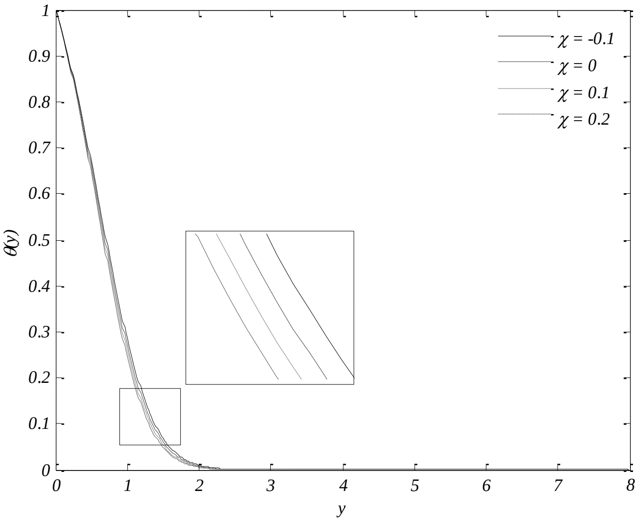

Fig. 4 Temperature profiles $\theta(y)$ against y for various values of χ when $\Pr=7, Le=10$ and $N_b=N_t=Ec=0.1$.

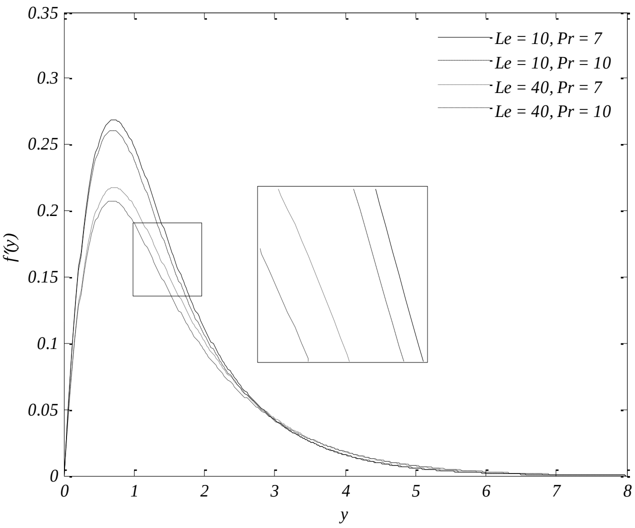

Fig. 5 Velocity profiles $f'(y)$ against y for various values of Pr and when $N_b=N_t=\chi=Ec=0.1.$

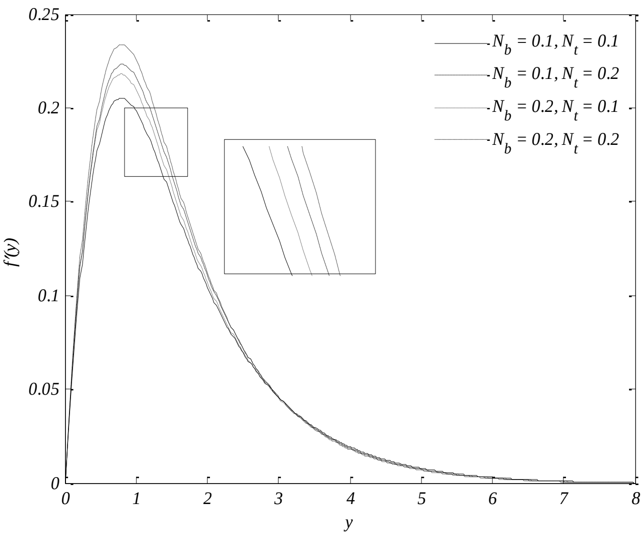

Fig. 6 Velocity profiles $f'(y)$ against y for various values of values of N_b and N_t when $\Pr=7,\ Le=10$ and $\chi=Ec=0.1.$

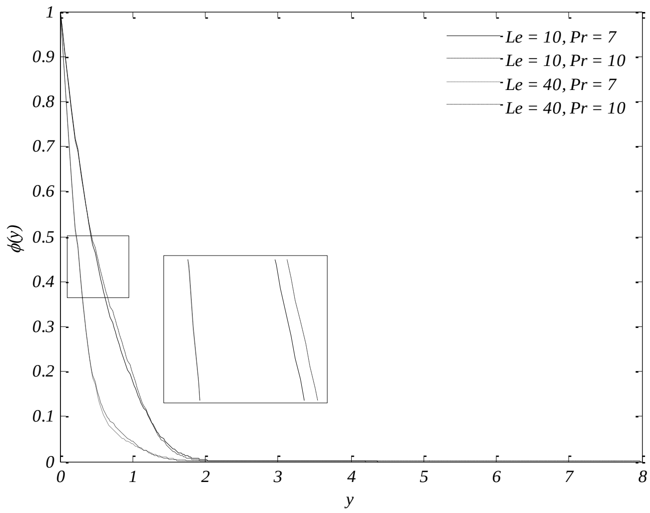

Fig. 7 Concentration profiles $\phi(y)$ against y for various values of Pr and Le when $N_b=N_t=\chi=Ec=0.1.$

Next, in discussing the concentration profiles $\phi(\eta)$, Fig. 7 shows concentration profile $\phi(\eta)$ at a stagnation region $(x=0)$ for various values of Le and Pr. It was observed that the increase of Le induced a reduction in $\phi(\eta)$. The increase in Pr gave a small increment in concentration and Pr effect was more pronounced with smaller value of Le. Further, the increase of N_b promoted the reduction of concentration boundary layer thickness while N_t did oppositely. According to Zaimi et al. (2014), the Brownian motion causes the nanoparticle deposition away from the fluid regime to the sphere surface which results in a decrease of the nanoparticle concentration boundary layer thickness. Meanwhile, N_t warms the fluid in the boundary layer and hence transmits energy onto nanoparticle which results the nanoparticle spreading away from the sphere surface. The concentration profiles $\phi(\eta)$ for various values of N_b and N_t are shown in Fig. 8.

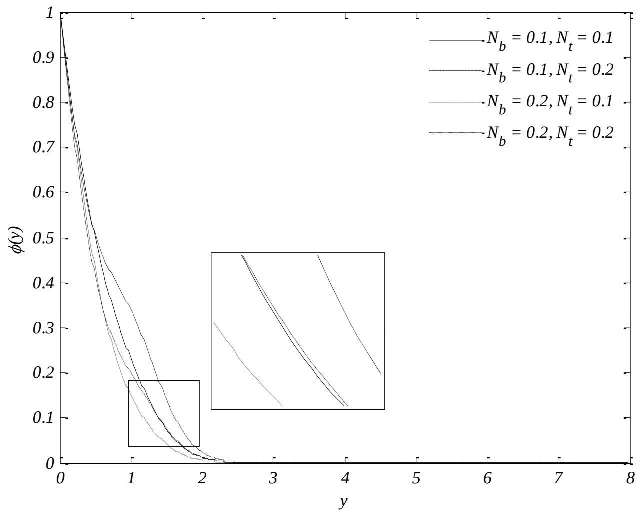

Fig. 8 Concentration profiles $\phi(y)$ against y for various values of N_b and N_t when $\Pr=7,\ Le=10$ and $\chi=Ec=0.1.$

In order to understand the fluid flow behavior and the parameter characteristic across the cylinder, Figs. 9-15 are illustrated. From the numerical computation, it is found that the fluid flow faces a separation boundary layer after $x=2\pi/3$, therefore the discussion is limited until $x=2\pi/3$ only. Figs. 9 and 10 show the variation of the reduced

Nusselt number $Nu_x Gr_x^{-1/4}$ for various values of N_b, N_t, Ec and Le, respectively. Both figures show a decreasing manner where $Nu_x Gr_x^{-1/4}$ decreased across the cylinder. Further, the increase of N_b, N_t, Ec and Le resulted in the decrease of $Nu_x Gr_x^{-1/4}$. This is due to higher values of N_b and N_t that subsequently result into higher volume of nanoparticles migrating away from the vicinity of the wall, and thus, reducing the value of $Nu_x Gr_x^{-1/4}$. Furthermore, from Fig. 9, the effect of Ec on $Nu_x Gr_x^{-1/4}$ was dominant as x increased. Meanwhile, from Fig. 10, it was suggested that the influence of N_b was more pronounced at the stagnation region $(x = 0)$.

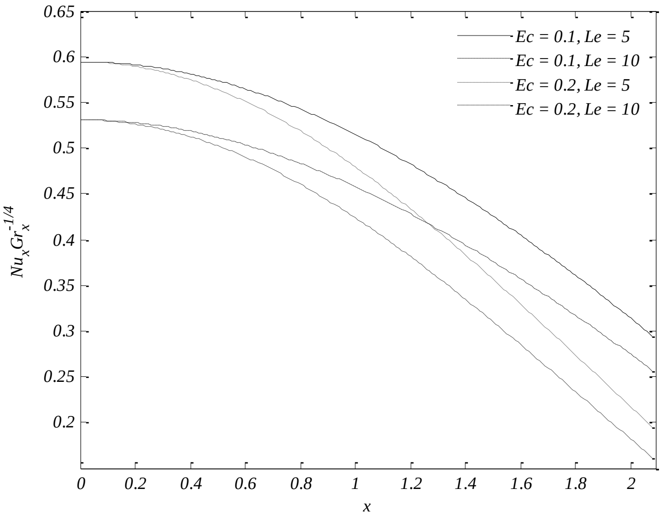

Fig. 9 Variation of $Nu_x Gr_x^{-1/4}$ against x for various values of Le and Ec when $N_b = N_t = \chi = 0.1$ and $\Pr = 7$.

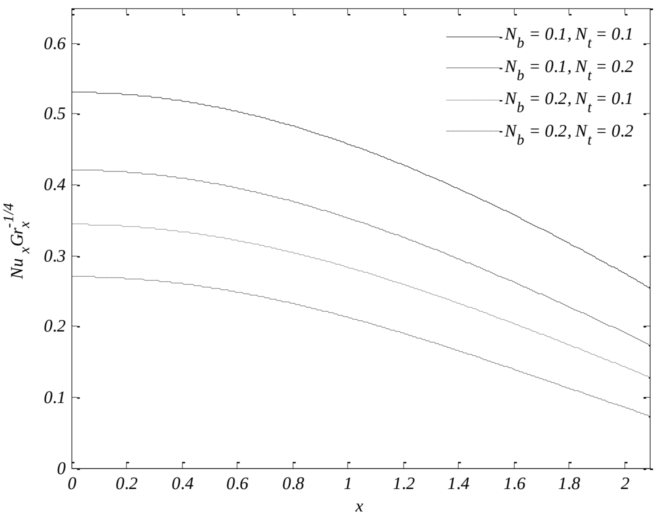

Fig. 10 Variation of $Nu_x Gr_x^{-1/4}$ against x for various values of values of N_b and N_t when $\Pr = 7,\ Le = 10$ and $\chi = Ec = 0.1$.

Next, Figs. 11-13 present the variation of the reduced Sherwood number $Sh_x Gr_x^{-1/4}$ for various values of Ec, N_b, N_t, Le and χ, respectively. It was found that the increase of parameters Ec, N_b, N_t, Le and χ resulted in the increase of $Sh_x Gr_x^{-1/4}$. Similar with Fig. 9, the changes in Ec have large effects on $Sh_x Gr_x^{-1/4}$ as x increased. The variation of $Sh_x Gr_x^{-1/4}$ across the cylinder in Figs. 12 and 13 was a decreasing function. This physically means that the mass transfer capability decreases as flow passes through sphere.

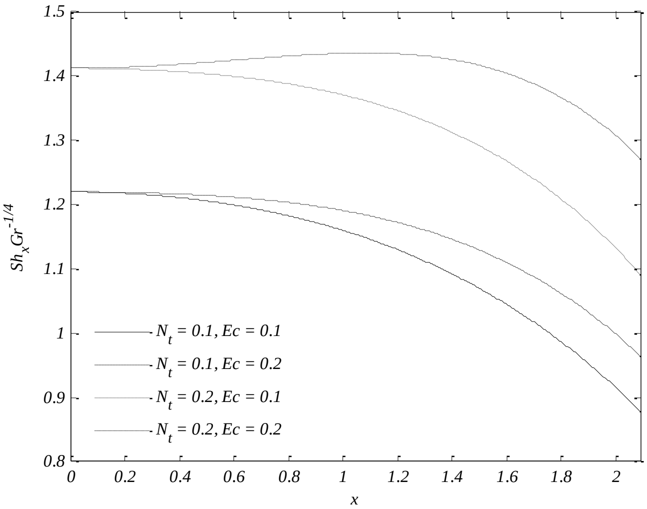

Fig. 11 Variation of $Sh_x Gr_x^{-1/4}$ against x for various values of values of Ec and N_t when $\Pr = 7,\ Le = 10$ and $N_b = \chi = 0.1$.

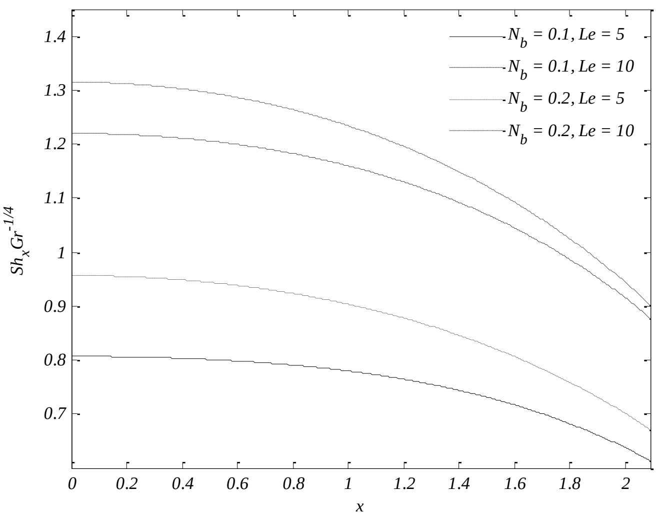

Fig. 12 Variation of $Sh_x Gr_x^{-1/4}$ against x for various values of values of Le and N_b when $Ec = N_t = \chi = 0.1$ and $\Pr = 7$.

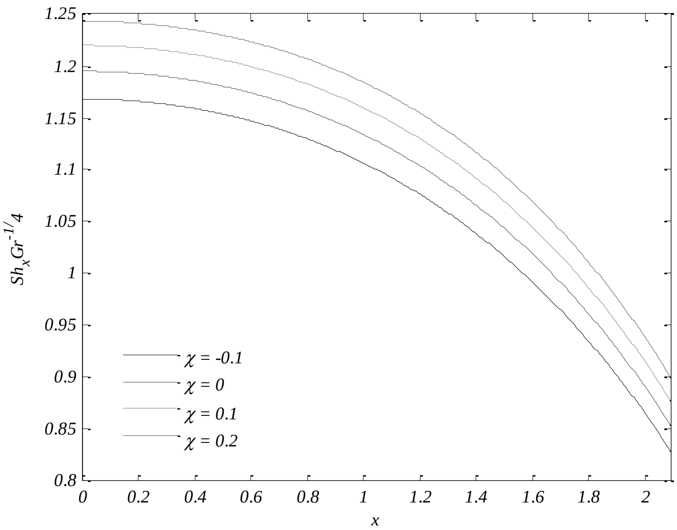

Fig. 13 Variation of $Sh_x Gr_x^{-1/4}$ against x for various values of χ when $\Pr = 7, Le = 10$ and $N_b = N_t = Ec = 0.1$.

Lastly, Figs. 14 and 15 present the variation of the reduced skin friction coefficient $C_f Gr_x^{1/4}$ for various values of Ec, Le and χ. It was ~~is~~ suggested that the effects of parameter discussed were unique at the stagnation region and became pronouncedly as x increased to the middle of the sphere. The increase of *Ec* and *Le* gave a small increment on $C_f Gr_x^{1/4}$.

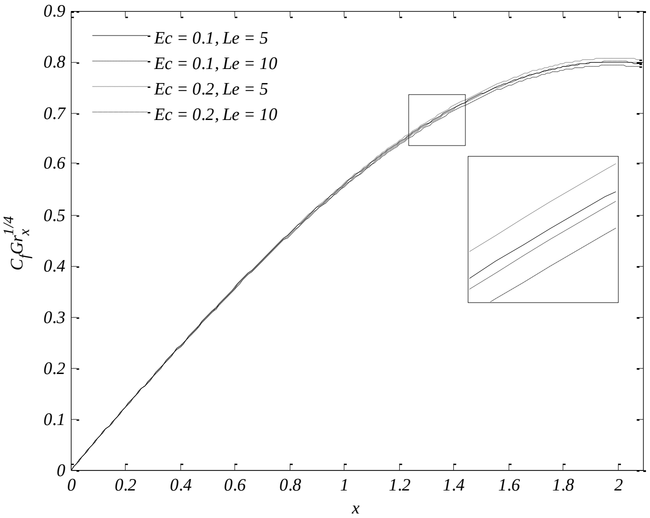

Fig. 14 Variation of $C_f Gr_x^{1/4}$ against x for various values of Le and Ec when $N_b = N_t = \chi = 0.1$ and $\Pr = 7$.

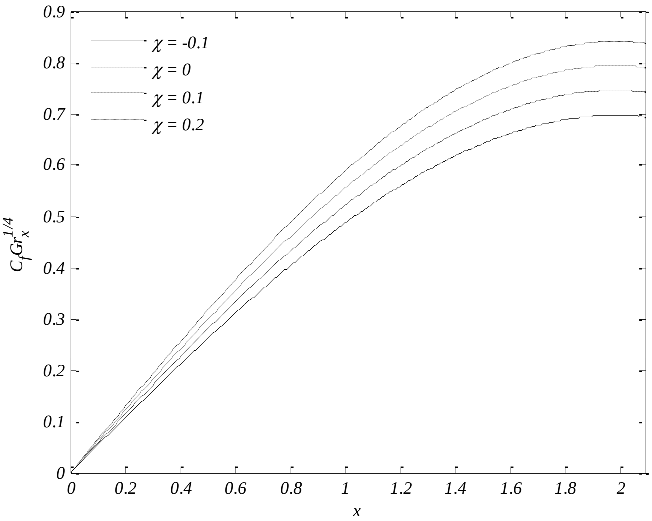

Fig. 15 Variation of $C_f Gr_x^{1/4}$ against x for various values of χ when $\Pr = 7, Le = 10$ and $N_b = N_t = Ec = 0.1$.

CONCLUSION

The problem of free convection boundary layer flow on a solid sphere immersed in a nanofluid in the presence of viscous dissipation effect has been solved numerically. The numerical results are obtained up to the end of the sphere.

As a conclusion, the increase of Prandtl number Pr results in the decrease of thermal boundary layer thickness and its velocity profile at the stagnation region. This is realistic since the increase of Pr indicates the reduction in the fluid ability to transmit heat and therefore, shortening its boundary layer thicknesses.

It is found that the reduced Nusselt number is a decreasing function accross the sphere body and the increase of Brownian motion parameter N_b, thermophoresis parameter N_t, Lewis number *Le* and the Eckert number *Ec* give a reduction on this physical quantity. In contrary with reduced Sherwood number, the quantities increase with the increase of Ec, N_b, N_t, Le and χ.

Furthermore, the effects of parameter discussed on reduced skin friction coefficient are unique at the stagnation region and become pronouncedly as flow passes through the middle of the sphere. From the numerical computation, it is found that the fluid flow faces separation boundary layer after $x = 2\pi / 3$, which agrees with similar cases reported previously.

ACKNOWLEDGEMENT

The authors would like to thank DRB-HICOM University of Automotive Malaysia and University Malaysia Pahang for the financial and facilities supports.

REFERENCES

Abdul Gaffar, S., Ramachandra Prasad, V., Keshava Reddy, E. & Anwar Bég, O. 2015. Thermal radiation and heat generation/absorption effects on viscoelastic double-diffusive convection from an isothermal sphere in porous media. *Ain Shams Engineering Journal*, 6(3), 1009-1030.

Abro, K. A., Rashidi, M. M., Khan, I., Abro, I. A. & Tassaddiq, A. 2018. Analysis of Stokes' second problem for nanofluids using modern approach of Atangana-Baleanu fractional derivative. *Journal of Nanofluids*, 7(4), 738-747.

Alkasasbeh, H. T., Salleh, M. Z., Tahar, R. M., Nazar, R. & Pop, I. 2014a. Free convection boundary layer flow on a solid sphere with convective boundary conditions in a micropolar fluid. *World Applied Sciences Journal*, 32(9), 1942-1951.

Alkasasbeh, H. T., Salleh, M. Z., Tahar, R. M., Nazar, R. & Pop, I. 2014b. Mixed convection boundary layer flow about a solid sphere with convective boundary conditions. *Wulfenia Journal*, 21(3), 386-404.

Amato, W. S. & Tien, C. 1972. Free convection heat transfer from isothermal spheres in water. *International Journal of Heat and Mass Transfer*, 15(2), 327-339.

Anwar, M. I., Shafie, S., Kasim, A. R. M. & Salleh, M. Z. 2016. Radiation effect on mhd stagnation-point flow of a nanofluid over a nonlinear stretching sheet with convective boundary condition. *Heat Transfer Research*, 47(9), 797-816.

Buongiorno, J. 2006. Convective transport in nanofluids. *Journal of Heat Transfer*, 128(3), 240-250.

Chiang, T., Ossin, A. & Tien, C. L. 1964. Laminar free convection from a sphere. *Journal of Heat Transfer*, 86(4), 537-541.

Gebhart, B. 1962. Effects of viscous dissipation in natural convection. *Journal of Fluid Mechanics*, 14(02), 225-232.

Gopmandal, P. P. & Bhattacharyya, S. 2011. Thermal buoyancy aided flow around a heated/cooled spherical particle. *Heat Transfer Research*, 42(8), 689-710.

Gul, A., Khan, I. & Makhanov, S. S. 2018. Entropy generation in a mixed convection Poiseulle flow of molybdenum disulphide Jeffrey nanofluid. *Results in Physics*, 9, 947-954.

Huang, M. J. & Chen, C. K. 1987. Laminar free convection from a sphere with blowing and suction. *Journal of Heat Transfer*, 109, 529-532.

Jafarpur, K. & Yovanovich, M. M. 1992. Laminar free convective heat transfer from isothermal spheres: A new analytical method. *International Journal of Heat and Mass Transfer*, 35(9), 2195-2201.

Jia, H. & Gogos, G. 1996. Laminar natural convection heat transfer from isothermal spheres. *International Journal of Heat and Mass Transfer*, 39(8), 1603-1615.

Kasim, A. R. M., Mohammad, N. F., Aurangzaib, A. & Shafie, S. 2013. Natural convection boundary layer flow past a sphere with constant heat flux in viscoelastic fluid. *Jurnal Teknologi*, 62(3), 27-32.

Khan, I. 2017. Shape effects of MoS2 nanoparticles on MHD slip flow of molybdenum disulphide nanofluid in a porous medium. *Journal of Molecular Liquids*, 233, 442-451.

Kho, Y. B., Hussanan, A., Mohamed, M. K. A., Sarif, N. M., Ismail, Z. & Salleh, M. Z. 2017. Thermal radiation effect on MHD flow and heat transfer analysis of Williamson nanofluid past over a stretching sheet with constant wall temperature. *Journal of Physics: Conference Series*, 890(1), 1-6.

Lien, F. S. & Chen, C. K. 1986. Analysis of forced convection micropolar boundary layer about a permeable sphere. *International Journal of Engineering Science*, 24(6), 991-999.

Mabood, F., Shateyi, S., Rashidi, M. M., Momoniat, E. & Freidoonimehr, N. 2016. MHD stagnation point flow heat and mass transfer of nanofluids in porous medium with radiation, viscous dissipation and chemical reaction. *Advanced Powder Technology*, 27(2), 742-749.

Mohamed, M. K. A. 2017. *Steady convective boundary layer flow in a nanofluid past on a bluff body with the viscous dissipation effect*. PhD Thesis, Universiti Malaysia Pahang.

Mohamed, M. K. A. 2018. *KELLER-BOX METHOD Partial differential equations in boundary layer flow of nanofluid.* DRB-HICOM University Publisher, Pekan.

Mohamed, M. K. A., Noar, N. A. Z., Salleh, M. Z. & Ishak, A. 2016. Free convection boundary layer flow on a horizontal circular cylinder in a nanofluid with viscous dissipation. *Sains Malaysiana*, 45(2), 289-296.

Mohamed, M. K. A., Sarif, N. M., Noar, N. A. Z., Salleh, M. Z. & Ishak, A. 2018. Mixed convection boundary layer flow on a horizontal circular cylinder in a nanofluid with viscous dissipation effect. *Malaysian Journal of Fundamental and Applied Sciences*, 14(1), 32-39.

Na, T. Y. 1979. *Computational methods in engineering boundary value problems*. Academic Press, New York.

Nalluri, S. V., Patel, S. A. & Chhabra, R. P. 2015. Mixed convection from a hemisphere in Bingham plastic fluids. *International Journal of Heat and Mass Transfer*, 84, 304-318.

Nazar, R., Amin, N., Grosan, T. & Pop, I. 2002a. Free convection boundary layer on an isothermal sphere in a micropolar fluids. *International Communications in Heat and Mass Transfer*, 29(3), 377-386.

Nazar, R., Amin, N., Groşan, T. & Pop, I. 2002b. Free convection boundary layer on a sphere with constant surface heat flux in a micropolar fluid. *International Communications in Heat and Mass Transfer*, 29(8), 1129-1138.

Salleh, M. Z., Nazar, R. & Pop, I. 2010. Modeling of free convection boundary layer flow on a solid sphere with Newtonian heating. *Acta Applicandae Mathematicae*, 112(3), 263-274.

Salleh, M. Z., Nazar, R. & Pop, I. 2012. Numerical solutions of free convection boundary layer flow on a solid sphere with Newtonian heating in a micropolar fluid. *Acta Meccanica*, 47, 1261-1269.

Ugur Akbulut, Rasim Volga. Ovali & Haydar Kucuk 2017. Viscous dissipation effects on entropy generation in heated vertical parallel-plate channels for mixed convection *International Journal of Energy*, 23(1), 1-17.

Wong, K. V. & De Leon, O. 2010. Applications of nanofluids: Current and future. *Advances in Mechanical Engineering*, 2010, Article ID 519659, 1-11.

Zaimi, K., Ishak, A. & Pop, I. 2014. Boundary layer flow and heat transfer over a nonlinearly permeable stretching/shrinking sheet in a nanofluid. *Scientific Reports*, 4, Article No. 04404, 1-8.

Zokri, S. M., Arifin, N. S., Mohamed, M. K. A., Kasim, A. R. M., Mohammad, N. F. & Salleh, M. Z. 2018. Influence of viscous dissipation on the flow and heat transfer of a Jeffrey fluid towards horizontal circular cylinder with free convection: A numerical study. *Malaysian Journal of Fundamental and Applied Sciences*, 14(1), 40-47.

Zokri, S. M., Arifin, N. S., Mohamed, M. K. A., Salleh, M. Z., Kasim, A. R. M. & Mohammad, N. F. 2017. Influence of radiation and viscous dissipation on magnetohydrodynamic Jeffrey fluid over a stretching sheet with convective boundary conditions. *Malaysian Journal of Fundamental and Applied Sciences*, 13(3), 279-284.